

## A Cat’s Eye View: Measuring Stellar Formation Rates in M94

MADÉLINE C. CASAS,<sup>1</sup> LUCAS A. PAUKER,<sup>1</sup> AND BILL. C. ROBERSON<sup>1</sup>

<sup>1</sup>*Stanford School of Humanities and Sciences, Department of Physics, Palo Alto, CA*

### ABSTRACT

Understanding the Stellar Formation Rate (SFR) of galaxies provides key insights into their formation and evolutionary lifetimes. Using the Stanford Student Observatory (SSO), we observe the SFR in M94, a Seyfert spiral galaxy. We define three distinct annular regions over which we compare and contrast SFR. We determine stellar formation activity by observation of H-II regions in the source. Over three hours at the SSO, we used the H $\alpha$  and R filters to determine photon flux from the LINER nucleus, the starburst region in the galaxy’s inner ring, and the galaxy’s outer ring using a scaled comparison of broad-spectrum to narrowband fluxes to perform our analysis. We optimized our observational time to achieve maximal signal-to-noise ratios and employ industry-standard error mitigation in calculations of the SFR in the region. We find a total SFR of  $3.08 \pm 7.49$  solar masses per year, a range in accordance with existing literature values for the total SFR. We also find that 67.1% of the SFR occurs in the inner ring, 32.9% occurs in the outer ring, and 0% occurs in the nucleus, and explore possible sources of discrepancy in our findings with the literature.

*Keywords:* Stellar Formation Rates — Starburst Galaxy — H-II Regions — Galaxy Evolution

### 1. INTRODUCTION

Understanding the process of star formation is one of the most insightful tools for understanding galaxy formation and evolution. By understanding the stellar formation rate (SFR) of a galaxy, we are given a window not only into that particular galaxy’s history, but also into how matter behaves at large scales.

#### 1.1. *H $\alpha$ emission flux as a probe for SFR*

One of the key indicators of recent stellar formation is the measurement of H $\alpha$  emissions from an optical target. H $\alpha$  is a prominent spectral line in the Balmer series for hydrogen. It is found in the visible light range with a wavelength of 656.46nm in vacuum. H $\alpha$  emissions occur when electrons in the hydrogen atom fall to the  $n = 2$  excited state, forming a far-red emission line in the Balmer series. H $\alpha$  emissions are notably prominent in areas of singly ionized hydrogen gas (H<sup>+</sup>) such as HII regions. The energy required for a hydrogen atom to transition from  $n = 1$  to  $n = 3$  is slightly less than the energy required to ionization. Observing H $\alpha$  emissions in a region indicates that it is highly probable that the energy required to cause ionization is present there.

Molecular clouds containing ionized hydrogen are called HII regions. One of the sources which can provide enough energy to create HII regions are young, massive ( $< 10M_{\odot}$ ) OB stars. These stars release UV radiation as they begin their lifetimes on the main sequence, ionizing the clouds of molecular hydrogen (H<sub>2</sub>) and exciting neutral hydrogen in the interstellar medium. The initial mass function (IMF) indicates that OB-type stars are the rarest to form in a given region, so it is inferred that their presence indicates the concurrent formation of many more small, dim stars. Furthermore, OB-type stars have fairly short lifetimes ( $< 20$  Myr). They will not sustain the requisite UV radiation pressure needed to create H $\alpha$  emission for long. Due to their short timescales for formation and dispersion, the presence of an HII region in a target is a sign that stellar formation of the rarest and most energetic stars is very recently underway (Kennicutt 1998). Research using H $\alpha$  emissions to understand recent ( $< 4 \times 10^6$  yrs) stellar formation rates (SFRs) in low-redshift HII regions is well-documented and ongoing in the field (Gavazzi, G. et al. (2006), Barth et al. (1994), James et al. (2004).)

#### 1.2. *Stellar formation in M94*

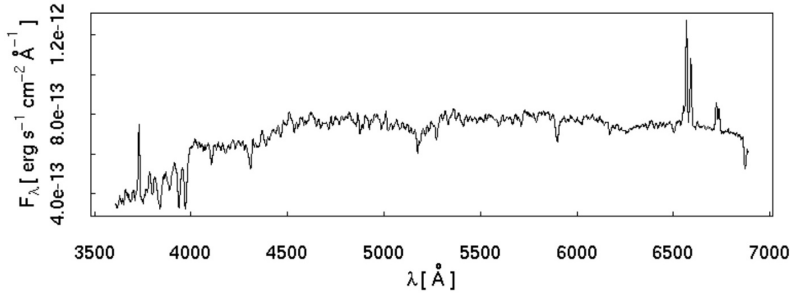


**Figure 1:** M94 Full Spectrum Chart illustrating  $H\alpha$  emission (Moustakas & Kennicutt 2006)

Our subject of study is M94 (NGC 4736), a spiral galaxy in the constellation Canes Venatici (RA 12h50m53.1s, DEC +41°07'14"). The source has an apparent magnitude of 8.2 (AAS Journals Team & Hendrickson 2016). M94 is an optimal target for several reasons. It contains an active galactic nucleus (AGN) which is classified as a Low Ionization Nuclear Emission Region (LINER), an inner starburst ring where there are relatively high amounts of stellar formation activity, and an outer ring which is also the site of subdued but relatively efficient star formation (Trujillo et al. (2009), Véron-Cetty & Véron (2006), Bosma et al. (1977), Rownd & Young (1999).) Further, the spiral is nearly face on from our vantage point, eliminating error associated high optical depth and dust blocking uniform observation of SFR in the source. Our research centers on the calculation of SFR in three regions of the target using observed  $H\alpha$  emission fluxes. The three regions are the AGN, the inner starburst ring, and the outer ring. The paper by Kennicutt (1998) reviews SFR in galaxies and provides methods for computation. One way to compute SFR is by using the luminosity and color. However, as demonstrated in (Kennicutt 1998), SFRs derived in this way are prone to systematic errors from many sources. A more accurate way to compute SFR is by using  $H\alpha$  data. Twite et al. (2012) use the following formula to measure SFR:

$$\text{SFR}(M_{\odot} \text{ yr}^{-1}) = 4.6 \times 10^{-42} L(H\alpha)(\text{erg s}^{-1}), \quad (1)$$

where  $L(H\alpha)$  represents the excess luminosity of the source in  $H\alpha$  above the continuum level, which is shown in figure 1 as the part of emission line over the continuum at the  $H\alpha$  wavelength. The constant in this equation comes from the Chabrier IMF.

In order to calculate luminosity from the flux  $F$ , we use the following formula:

$$L = 4\pi d^2 F, \quad (2)$$

where  $d$  is the distance to M94. We calculated the flux from our observational data. In order to determine the distance  $d$ , we can look to existing literature ((Walker 2017), (Herrmann et al. 2008)). In our project, we separate our analysis into three annuli in order to distinguish different SFR in the galactic nucleus, inner starburst ring, and outer ring. We performed error propagation on our flux calculations and have fit error bars to our final data.

## 2. OBSERVATIONS AND DATA REDUCTION

### 2.1. SSO Observing Specifics

Observations were gathered at the Stanford Student Observatory on April 28, May 11, and May 18, 2022, totaling in 7,500s of data collected using the  $H\alpha$  filter and 330s using the R-Band filter. Filter specifics can be found in table 1 below. We employed use of the 24" cassegrain-focus telescope and CCD camera. We chose to alternate our intervals of data collection in  $H\alpha$  and R to avoid differences across filters due atmospheric changes during the observational period. On our first night of observing we took 60s exposures in R and  $H\alpha$ . For the remaining nights we switched to 15 second exposures in R band taken between intervals of 10 exposures of 60s each in  $H\alpha$ . Data collection as broken into nightly observing sessions can be found in table 2.

### 2.2. Data Reduction

There were three steps we took to reduce our data before doing our analysis: calibrating the images, aligning the images, and coadding the images. To calibrate the images, we took dark, bias, and flat frames. For each image, we used the following calibration formula:

| Filter     | $\lambda(\text{\AA})$ | FWHM |
|------------|-----------------------|------|
| R          | 6584                  | 1380 |
| H $\alpha$ | 6563                  | 30   |

**Table 1:** Information for filters used in observation. Note  $\lambda$  in column two is the midpoint of the filter wavelength.

| Observing Date | Exposure Time (R) | Exposure Time (H $\alpha$ ) |
|----------------|-------------------|-----------------------------|
| 4/28/22        | 180s              | 1500s                       |
| 5/11/22        | 90s               | 3600s                       |
| 5/18/22        | 60s               | 2400s                       |

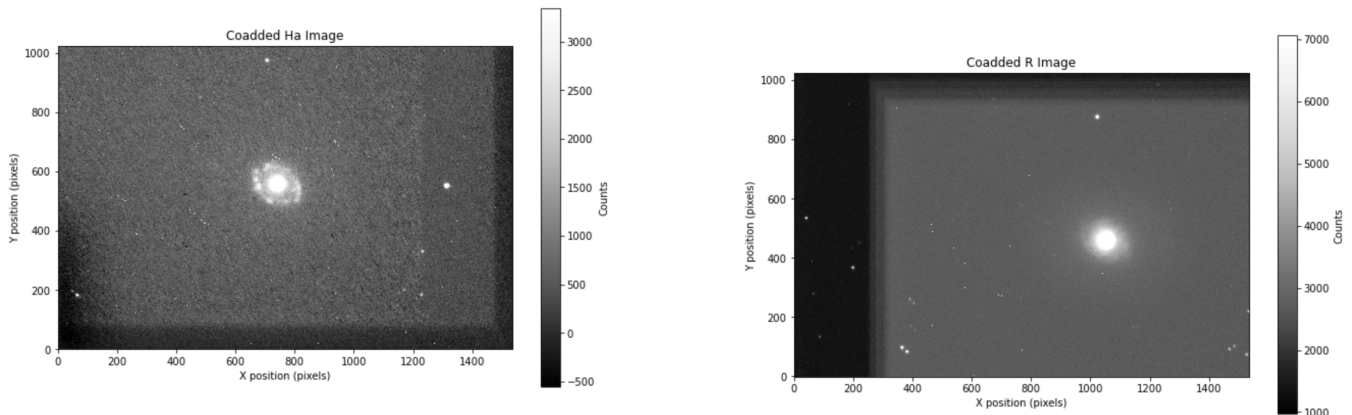
**Table 2:** Observation time nightly total exposure times and filter allocation

$$S = m(R - B - tD)/F, \quad (3)$$

where  $R$  is a matrix of the values of the uncalibrated image,  $B$  is a matrix of the average bias frame values,  $D$  is a matrix of the average dark frame values,  $F$  is a matrix of the average flat frame values,  $m$  is the median value of  $F$ ,  $t$  is the exposure time, and  $S$  is the calibrated science image.

To align the images, we used ASTAP's manual alignment feature. This required us to locate the same reference star in every calibrated frame and based on the location of the reference star, ASTAP aligned the images. For this process, we were only able to use a single star as a reference star since there was only one star that was visible across all the frames we had.

The last step of our data reduction was to coadd the images. This consisted of us adding the pixel values for all the aligned images in each band. After this step, we were left with two frames: one coadded H $\alpha$ -band frame and one coadded R-band frame. Figure 2 shows the two coadded images.



(a) Coadded image of the H $\alpha$  band data. We can see the galactic nucleus and the starburst ring.

(b) Coadded image of the R band data.

**Figure 2:** Coadded images in H $\alpha$  and R bands.

### 3. METHODS AND RESULTS

#### 3.1. Aperture Photometry

The first step of our data analysis was to get the instrumental flux of our target as well as a reference star in both the H $\alpha$  and R bands. For our reference star, we used GPM 192.726069+41.052152, which was cataloged by Rybka & Yatsenko. We chose this star since it was the only star visible in every frame we had. For our aperture photometry, we used an elliptical aperture. This is because M94 has an elliptical shape, and using an elliptical aperture allows us to perform calculations on different regions of the galaxy with greater accuracy.

| Emission Line | Wavelength (Å) | Integrated Emission Line Flux |
|---------------|----------------|-------------------------------|
| OI            | 6300           | 163.0±27.0                    |
| H $\alpha$    | 6563           | 6760.0±270.0                  |
| NII           | 6584           | 3640.00±150.0                 |

**Table 3:** Integrated Emission Flux for M94 (Moustakas et. al 2006). Note that column three is in units of  $10^{-15}$  ergs  $s^{-1} \text{ cm}^{-2}$

### 3.2. Differential Photometry

After using aperture photometry to determine the instrumental flux for M94 as well as the reference star in both the H $\alpha$  and R band, we used differential photometry to calibrate the fluxes. The first step was to convert the instrumental flux into magnitude using the following formula:

$$m_{\text{ref,R}} = -2.5 * \log_{10}(F_{\text{ref,R}}); \quad m_{\text{M94,R}} = -2.5 * \log_{10}(F_{\text{M94,R}}); \quad m_{\text{M94,H}\alpha} = -2.5 * \log_{10}(F_{\text{M94,H}\alpha}), \quad (4)$$

where  $m_{\text{ref,R}}$ ,  $m_{\text{M94,R}}$ , and  $m_{\text{M94,H}\alpha}$  are the instrumental magnitudes of the reference star in the R band, M94 in the R band, and M94 in H $\alpha$ , respectively. Similarly,  $F_{\text{ref,R}}$ ,  $F_{\text{M94,R}}$ , and  $F_{\text{M94,H}\alpha}$  are the instrumental fluxes of the reference star in the R band, M94 in the R band, and M94 in H $\alpha$ , respectively. We knew the true apparent magnitude of our reference star  $m_{\text{ref,true}}$  in the R band from a catalog (Rybka & Yatsenko 1997). We then defined  $\Delta m$  as the correction that we must make for differential photometry:

$$\Delta m = m_{\text{ref,true}} - m_{\text{ref,R}}. \quad (5)$$

Using  $\Delta m$ , we conduct differential photometry to get the calibrated magnitudes for M94 in the R band and H $\alpha$  band with this formula:

$$m_{\text{cal,M94,H}\alpha} = m_{\text{M94,H}\alpha} + \Delta m; \quad m_{\text{cal,M94,R}} = m_{\text{M94,R}} + \Delta m, \quad (6)$$

where  $m_{\text{cal,M94,R}}$  and  $m_{\text{cal,M94,H}\alpha}$  are the calibrated magnitudes in the R and H $\alpha$  bands, respectively. Using this calculation, we find that  $m_{\text{cal,M94,R}} = 8.57 \pm 0.00239$  and  $m_{\text{cal,M94,H}\alpha} = 12.46 \pm 0.00240$ .

### 3.3. Removing Nitrogen Emission Line

An important part of isolating the signal associated with the  $L(H\alpha)$  emission line (6563Å) is removing the contributions associated with the nearby Nitrogen emission line (6584Å). In order to isolate the presence of nitrogen flux in our gathered H $\alpha$  observations, we must understand relative emission line fluxes between NII and H $\alpha$  in M94. We reference spectroscopic data collected by Moustakas & Kennicutt (2006). In table 3, we include data from this paper for M94. Burbidge & Burbidge (1962) find that the relative presence of H $\alpha$  to NII to be around 3 in the inner ring, diminishing to around a 1:1 ratio in the nuclear bulge. However, the peak of this Nitrogen line is toward the edge of the filter, where transmission is 30%. Therefore, in correcting the luminosities we assume that this ratio will be 3 times greater. To account for the potential overlap of H $\alpha$  emissions and the Nitrogen line in our results we scale our results by a factor of 0.9 in the inner and outer rings and 0.75 in the nucleus. When calculating SFR for the whole galaxy, we must choose how to combine these values. While the literature suggests that most of the luminosity in H $\alpha$  comes from the nucleus, our answer suggests that the nucleus has a relatively low amount of stellar formation. Because of this, if we use the correction factor from the nucleus for the entire galaxy, we find a negative SFR, likely due to the same error that resulted in measuring a higher SFR in the inner and outer rings. Because of this, we correct with the 0.9 factor for the entire galaxy, but report the results both before and after this correction.

### 3.4. Luminosity Calculation

After calculating the calibrated magnitudes, we then calculate the luminosity in two different ways. The first method involves unit conversions and equation 2. The second method involves using absolute magnitudes. We will describe both methods.

For the first method, we first convert calibrated magnitudes into fluxes. The formula to convert calibrated magnitude  $m$  into flux  $F$  is:

$$F = 10^{-m/2.5}. \quad (7)$$

This allows us to find the calibrated magnitudes for M94 in the R and H $\alpha$  bands. We then calculate the luminosity in the R and H $\alpha$  bands by using equation 2. For the distance to M94 that we need for the equation, we use the result from (Herrmann et al. 2008). Using this method, we found that the luminosity in the R band is  $1.11 * 10^{33} \pm 6.53 * 10^{26}$  ergs/s and the luminosity in the H $\alpha$  band is  $3.01 * 10^{31} \pm 6.56 * 10^{26}$  ergs/s before the correction for the Nitrogen line, and  $2.79 * 10^{31} \pm 5.90 * 10^{26}$  ergs/s after correction for the Nitrogen line.

The second method for computing luminosity involves using absolute magnitudes. The formula to convert calibrated magnitude  $m$  into absolute magnitude  $M$  is:

$$M = m - 5 * \log_{10}(d) + 5, \quad (8)$$

where  $d$  is the distance to M94. This allows us to find the absolute magnitudes for M94 in the R and H $\alpha$  bands. We then use the following formula to calculate luminosity  $L$  from absolute magnitude  $M$ :

$$L = L_{\odot} * 10^{M_{\odot} - M}, \quad (9)$$

where  $L_{\odot}$  is the luminosity of the sun and  $M_{\odot}$  is the absolute magnitude of the sun. Using this method, we find that the luminosity in the R band is  $2.95 * 10^{43} \pm 4.81 * 10^{42}$  ergs/s and the luminosity in the H $\alpha$  band is  $8.20 * 10^{41} \pm 1.34 * 10^{41}$  ergs/s before the Nitrogen line correction, and  $7.38 * 10^{41} \pm 1.21 * 10^{41}$  ergs/s after the correction.

The luminosity calculations for these two methods differ by a factor of  $10^{10}$ . Clearly, this factor is huge. However, the ratio of luminosities in each of the two bands is very close (34 for both methods). We believe the first luminosity calculation contains an error. We report results following from both calculations, however we are more confident in the second one due to its increased agreement with literature values. Therefore, in the following sections, when referring to the luminosity we are referring to the second (larger) values, unless otherwise stated.

### 3.5. SFR Calculation

Once we compute the luminosities in both the R and H $\alpha$  bands, we can then turn to the SFR calculation. The first step is to calculate the excess H $\alpha$  luminosity  $L_{\text{final}}$  by subtracting the R band luminosity  $L_{\text{R}}$  from the H $\alpha$  luminosity  $L_{\text{H}\alpha}$ . However, there is a scaling factor  $\Delta W$  such that,

$$L_{\text{final}} = L_{\text{H}\alpha} - L_{\text{R}} / \Delta W. \quad (10)$$

We calculate  $\Delta W$  by dividing the integrated transmission curve for the R filter by the integrated transmission curve for the H $\alpha$  filter. Our calculated value for  $\Delta W$  was 43.89 by using the transmission data from the Johnson-Cousins filters. We then plug  $L_{\text{final}}$  into equation 1 to get the final SFR calculation. We find an SFR of  $6.85 \pm 7.96$  solar masses per year before correcting for the Nitrogen line and an SFR of  $3.08 \pm 7.49$  solar masses per year after correcting.

Initially, we considered employing the second of the two constants to determine our SFR as it had been referenced in one of our foundational sources, Kennicutt (1998), and replicated many subsequent times in the literature. We have since moved to adopt the IMF constant referenced in Twite et al. (2012), which adopts an adjustment in accordance with Chabrier (2003) which presents an updated understanding of the IMF from the Salpeter model used in earlier papers. The Chabrier IMF is particularly of use for early-type spiral galaxies such as M94.

### 3.6. SFR in Different Regions of M94

We are interested in finding the SFR in three distinct regions of M94: the galactic nucleus, the inner starburst ring, and the outer ring. To find the SFR in these regions, we use annulus-shaped apertures formed by subtracting elliptical apertures. We find that the SFR for the galactic nucleus is negligible. The SFR for the inner starburst region is  $4.51 \pm 3.06$  solar masses per year before Nitrogen correction and  $2.98 \pm 2.86$  solar masses per year after the correction. Lastly, the SFR for the outer ring is  $3.06 \pm 2.13$  solar masses per year before Nitrogen correction and  $2.00 \pm 1.99$  solar masses per year after Nitrogen correction. Therefore, we find that about 0% of SFR occurs in the nucleus, 67.1% occurs in the inner ring, and 32.9 % occurs in the outer ring. We notice that these numbers do not perfectly add up to the total SFR. This is because the SFR in the nucleus is actually slightly negative. Possible reasons for this error are brought up in the discussion section.

### 3.7. Error Propagation

At each calculation step, we employ error propagation to understand the uncertainty in our measurements. Most of these steps employ the basic Taylor approximation formula for error propagation, or the steps involve simply adding independent errors in quadrature. Two steps differ from these simple rules: when calculating the flux of our object, we employ the standard error calculation: we include the error from photon noise from the object and background, read noise, and the dark current. Since we perform this calculation on coadded images, we have to take into account that our data have two sets of darks and biases which apply to different exposures.

The other unique step is when calculating the difference between luminosities. In principal, these luminosities can be correlated, and so we cannot simply add the error in quadrature. We must also include a covariance term, as shown below.

$$\sigma_{\text{diff}}^2 = \sigma_{H\alpha}^2 + \sigma_R^2 - 2 * \frac{Cov}{\Delta W} \quad (11)$$

To estimate this covariance, we calculate the luminosity in Ha and R for each exposure, and use the definition of covariance to obtain an estimate. Specifically, we calculate

$$Cov = \frac{\sum_{i=1}^{n_{H\alpha}} \sum_{j=1}^{n_R} L_{H\alpha,i} * L_{R,j}}{n_{H\alpha} * n_R} - \frac{\sum_{i=1}^{n_{H\alpha}} L_{H\alpha,i}}{n_{H\alpha}} \frac{\sum_{j=1}^{n_R} L_{R,j}}{n_{R,j}} \quad (12)$$

where  $n_x$  is the number of exposures in the  $x$  band, and  $L_{x,k}$  is the luminosity in the  $x$  band from the  $k$ th exposure. We find this covariance to be over 10 orders of magnitude smaller than the variance of our measurements, and thus contributes minimally.

One important note is that our error in SFR is the same order of magnitude as our SFR. This large error seems to come primarily from the differential photometry step, as we only use one reference star to calibrate our magnitudes. As an avenue for future study, we could thus be careful to keep multiple reference stars in each exposure to ensure we can decrease error in our differential photometry step.

#### 4. DISCUSSION

Our estimates of SFR in the inner and outer ring of M94 are greater than that of the literature, and our results underestimate the SFR in the nucleus. We also find that the distribution of stellar formation is disproportionately centered in the inner ring in comparison to literature values. While we estimate that the inner ring is responsible for 67.1% of the total SFR of M94, Trujillo et al. (2009) find that this region contributes only 13% of the total stellar formation rate. Instead, they suggest that the bulk of stellar formation occurs in the central bulge, at a rate of 0.75 Solar masses per year. In further contrast, they find a smaller contribution to overall SFR from the outer disk than our findings suggest, 14% compared to our 32.9%. The findings from this paper suggest that the majority of contributions to total SFR come from the galactic nucleus, in stark contrast to our results.

These differences in our values as they compare to the literature may originate from several sources. First, Trujillo et al. (2009) utilize significantly deeper exposures than in our methodology, with observing times totaling over 33,300 seconds to compose single images. This procedure allows them to achieve a much more advantageous ratio of signal to noise in their results. Further, they employ seventeen different filters, allowing them to get a much fuller picture of SFR in the source.

It is likely that our over-estimate of SFR in the outer region of M94 was augmented by noise which we were not able to quiet in our analysis, simply by nature of the limitations of our observing constraints across a three hour total period. Indeed, it is not possible to optically distinguish the outer disk from the background sky in either of our coadded images. Excess noise in the region of the outer disk in both R-band and H $\alpha$  may have caused us to wrongfully attribute more stellar formation activity to this region than is actually there.

Our under-estimate of SFR in the central region of the galaxy may be attributed to other weaknesses in our methodology. Assuming the oldest stars in the galaxy are concentrated at the center of the M94, it is reasonable to expect much more red light sources there than the H $\alpha$  emitting ones associated with O and B type stars. This discrepancy may account for our underestimate of the stellar formation there. Perhaps there are other issues associated with attenuation from dust and other sources in the galactic bulge which we originally assumed to be negligible due to the low optical depth of our target.

An interesting point of reference between to our low SFR in the bulge are results from Muoz-Tun et al. (2004), showing very little H $\alpha$  flux for the nuclear region in comparison to flux associated with NII. It is possible that this is further evidence to the idea that there may be star formation in that region which is not easily traced by H $\alpha$  emissions.

## 5. CONCLUSIONS

We used the instruments at the Stanford Student Observatory over the course of Spring Quarter 2022 to measure the stellar formation rates overall and in three annuli of M94. We determine a total galactic SFR of  $4.49 \pm 7.67$  solar masses per year after correcting for Nitrogen. Accounting for error, this measurement does encapsulate the accepted literature SFR value of approximately  $1 M_{\odot}$  per year.

In calculating SFR measurements in elliptical annuli, we find that i) SFR for the galactic nucleus is negligible, ii) SFR for the inner starburst region is  $2.98 \pm 2.86$  solar masses per year after Nitrogen correction, and iii) SFR for the outer ring is  $2.00 \pm 1.99$  solar masses per year after Nitrogen correction.

Comparison to existing literature and error propagation suggest that there remain significant discrepancies between our measured values and the actual SFR in the galaxy, most notably in our understanding of SFR in the galactic nucleus. We believe these discrepancies may be attributable to attenuation of  $H\alpha$  emissions in the bulge of the galaxy or issues related to the limited presence of OB stars in the older star forming regions at the center of the galaxy.

We are happy to thank the incredible teaching team for Stanford's Physics 100 course, Prof. Steven Allen and the Teaching Assistants Richie and Andrew, for their continued encouragement, patience, and generous donations of time and energy to each team. Their guidance was a key factor in allowing our project to be carried out smoothly. Special thanks to them for showing us the ropes of the SSO and inspiring us every week.

## APPENDIX

All members of group contributed to every aspect of the project to at least some degree. Much of the problem solving and bug fixing was done as a team during group work sessions. However, certain team members of course took the lead on various project roles. The below table details which team members led the major sections of the project.

| Lucas                        | Madeline                        | Bill                           |
|------------------------------|---------------------------------|--------------------------------|
| Luminosity & SFR Calculation | Presentation & Report           | Reduction & Photometry Scripts |
| Differential Photometry      | Nitrogen Line Correction        | Error Propagation              |
| Data Alignment               | Astrometry & Ellipse Parameters | Script Debugging               |

## REFERENCES

- AAS Journals Team, & Hendrickson, A. 2016, doi: [10.5281/zenodo.168228](https://doi.org/10.5281/zenodo.168228)
- Barth, C. S., Cepa, J., Vilchez, J. M., & Dottori, H. A. 1994, AJ, 108, 2069, doi: [10.1086/117219](https://doi.org/10.1086/117219)
- Bosma, A., van der Hulst, J. M., & Sullivan, W. T., I. 1977, A&A, 57, 373
- Burbidge, E. M., & Burbidge, G. R. 1962, ApJ, 135, 694, doi: [10.1086/147313](https://doi.org/10.1086/147313)
- Chabrier, G. 2003, PASP, 115, 763, doi: [10.1086/376392](https://doi.org/10.1086/376392)
- Gavazzi, G., Boselli, A., Cortese, L., et al. 2006, A&A, 446, 839, doi: [10.1051/0004-6361:20053843](https://doi.org/10.1051/0004-6361:20053843)
- Herrmann, K. A., Ciardullo, R., Feldmeier, J. J., & Vinciguerra, M. 2008, The Astrophysical Journal, 683, 630, doi: [10.1086/589920](https://doi.org/10.1086/589920)
- James, P., Shane, N., Beckman, J., et al. 2004, Astronomy and Astrophysics, 414, 23, doi: [10.1051/0004-6361:20031568](https://doi.org/10.1051/0004-6361:20031568)
- Kennicutt, Robert C., J. 1998, ARA&A, 36, 189, doi: [10.1146/annurev.astro.36.1.189](https://doi.org/10.1146/annurev.astro.36.1.189)
- Moustakas, J., & Kennicutt, Robert C., J. 2006, ApJS, 164, 81, doi: [10.1086/500971](https://doi.org/10.1086/500971)
- Muoz-Tun, C., Caon, N., & Aguerri, J. A. L. 2004, The Astronomical Journal, 127, 58, doi: [10.1086/380610](https://doi.org/10.1086/380610)
- Rownd, B. K., & Young, J. S. 1999, AJ, 118, 670, doi: [10.1086/300957](https://doi.org/10.1086/300957)
- Rybka, S. P., & Yatsenko, A. I. 1997, Kinematika i Fizika Nebesnykh Tel, 13, 70
- Trujillo, I., Martinez-Valpuesta, I., Martínez-Delgado, D., et al. 2009, ApJ, 704, 618, doi: [10.1088/0004-637X/704/1/618](https://doi.org/10.1088/0004-637X/704/1/618)
- Twite, J. W., Conselice, C. J., Buitrago, F., et al. 2012, Monthly Notices of the Royal Astronomical Society, 420, 1061, doi: [10.1111/j.1365-2966.2011.20057.x](https://doi.org/10.1111/j.1365-2966.2011.20057.x)
- Véron-Cetty, M. P., & Véron, P. 2006, A&A, 455, 773, doi: [10.1051/0004-6361:20065177](https://doi.org/10.1051/0004-6361:20065177)

283 Walker, R. 2017, *Extragalactic Objects* (Cambridge  
284 University Press), 149–164,  
285 doi: [10.1017/9781316694206.027](https://doi.org/10.1017/9781316694206.027)